



## **FABRICATION AND ASSESSMENT OF SiC/Al<sub>2</sub>O<sub>3</sub> NANO-FILLER IMPACT ON THE PHYSICAL, FLAMMABILITY AND MECHANICAL PROPERTIES OF E-GLASS FIBER REINFORCED EPOXY HYBRID COMPOSITES**

**Mr. Pankaj Pradhan**, Research Scholar, Department of Mechanical Engineering, Jagannath University, Jaipur, Rajasthan, India-302015.

**Mr. Rakesh Kumar**, Assistant Professor, Department of Mechanical Engineering, Jagannath University, Jaipur, Rajasthan, India-302015.

**Mr. Rahul Sharma**, Research Scholar, Department of Mechanical and Industrial Engineering Engineering, IIT Roorkee, Roorkee, Uttarakhand, India-247667.

### **ABSTRACT**

The current investigation focuses on the influence of the presence of SiC and Al<sub>2</sub>O<sub>3</sub> particles at different weight percentages (from 0 wt. % to 6 wt. %) in epoxy-based composites fabricated by compression molding on their physical and mechanical characteristics. In order to comprehend the physical and mechanical characteristics as per ASTM standards of ceramics reinforced hybrid composites, this research specifically assessed the density, moisture content, and dimensional stability, tensile, flexural, impact and hardness of the composites. Factorgraphy analysis of tensile and flexure specimens performed through SEM. Following the execution of three replicates for each experiment, the study explores reduction in the density of the composites, the impact of immersion time in water and the variation in ceramics weight percentage on the dimensional stability of these composites. The maximum values for tensile strength (172.36±8.028 MPa), flexural strength (164.493±9.918 MPa), impact (24.2±1.643J/m) and hardness (77.3± 1.702 HSN) were observed at 4 wt% of SiC/Al<sub>2</sub>O<sub>3</sub>, which make the composite suitable for automobile parts and sports goods applications.

### **Keywords:**

Glass Fiber, Epoxy resin; SiC-Al<sub>2</sub>O<sub>3</sub>, Compression molding, Flammability, Physical and Mechanical properties.

### **I. Introduction**

In today's landscape, the utilization of fiber-reinforced polymer matrix composite materials has become widespread across a diverse range of applications, including aerospace, automotive, construction, and the sporting industries. These composites are favored for their exceptional attributes, such as high specific stiffness, specific strength, low thermal expansion, robust fatigue resistance, and suitability for the production of complex shapes. Composite materials typically encompass a matrix, which is commonly a polymer, along with fibers and fillers. Among these components, glass fibers stand out as the predominant choice in polymer matrix composites. This preference arises from their cost-effectiveness and favorable mechanical properties [1].

Ertan Kosedag et al. conducted an assessment of mechanical properties of CFRP composite fabricated by vacuum fusion technique with reinforcement of silicon carbide (SiC, 0.5, 1.0, 2.0 wt.%) and Graphene (Gr, 0.5, 1.0, 2.0 wt.%) nanoparticles. In their study, the independent variable 0.5 wt. % SiC reinforced CFRP composite exhibited better tensile and flexural strength other composites [1]. S.M. Shahabaz et al. conducted an assessment of mechanical properties of CFRP composite fabricated by vacuum in fusion technique with reinforcement of silicon carbide (SiC, 1.0, 1.25, 1.75, 2.0 wt.%) and alumina (Al<sub>2</sub>O<sub>3</sub>, 0.5, 1.25, 1.75, 2.0 wt.%) nanoparticles. In this study, maximum tensile noted at 1.75 wt. % Al<sub>2</sub>O<sub>3</sub> and 1.25 wt. % SiC. Using Barcol hardness tester, maximum hardness obtained at similarly compositions [2]. S. Sathish et al. investigated the mechanical characteristics of Al<sub>2</sub>O<sub>3</sub>/SiC-incorporated flax fiber-reinforced epoxy composite fabrication using compression molding. The influence of 8-2 wt% (SiC- Al<sub>2</sub>O<sub>3</sub>) ceramic exhibited maximum tensile, flexural, ILLS, and impact strength [3]. M.D. Kiran et al. carried out a comparative study on the mechanical characteristics of



GF-reinforced epoxy composites incorporated with SiC/TiO<sub>2</sub> and SiC/Al<sub>2</sub>O<sub>3</sub>, which fabricated using hand layup process. The findings indicate that the GFRP composite with 6 wt.% SiC/Al<sub>2</sub>O<sub>3</sub> exhibits the highest flexural, impact, and tensile strength, attributed to the high hardness and fracture toughness of SiC particles in the composite [4]. Narinder Singh et al. conducted an investigation into the mechanical characteristics of Al<sub>2</sub>O<sub>3</sub>/SiC-reinforced HDPE composites using FDM filament followed by screw extrusion for rapid tooling application. The results indicated improved mechanical strength attributed to the effective embedding of ceramic particles in the final specimen produced through FDM filament [5]. Olajide Tunmilayo Sanya et al. conducted a comparative analysis on the mechanical properties of SiC-reinforced epoxy composites with finer and coarser particulates, fabricated through an open mold casting process. The findings revealed that incorporating small particulate SiC (< 45 μm) led to superior mechanical characteristics in flexural, compressive, and hardness aspects across all volume fractions. Notably, the flexural properties of the composite samples exhibited a decrease with rising filler loading, while compressive strength and hardness demonstrated an increase with higher particulate volume fractions [6].

GFRP composites filled with fly ash exhibited improved dimensional stability after one day of immersion in water. [7]. Sharma and Gupta conducted a study on the chemical resistance of an epoxy resin composite reinforced with E-glass fibers and particulate fillers of aluminum oxide and silicon carbide. Their study indicated that composites filled with 2 wt. % of Al<sub>2</sub>O<sub>3</sub>/SiC (in a 1:1 ratio) displayed robust chemical resistance when exposed to acids and solvents for a duration of one day [8]. Sharma et al. observed that the epoxy composite filled with CSP/WSP (1:1) exhibited a reduction in dimensional stability as the quantity of particulates increased over time during immersion in water [9]. Nitin mukesh mathur et al. found that the composites composed of sugarcane bagasse fiber and chicken feather fiber, using polylactic acid as a matrix, experienced a decrease in dimensional stability as the quantity of particulates increased over time during immersion in water [10].

Previous studies have indicated that the physical and mechanical characteristics of ceramic GFRE composites depend on factors such as particle size, the loading of particles and the adhesion at the particle-matrix interface. However, there is a scarcity of research in the literature regarding the physical behaviors of ceramic GFRE composites with micron-scale particle content. Consequently, this current study aims to investigate the physical and mechanical behavior of epoxy matrices with micron-sized SiC-Al<sub>2</sub>O<sub>3</sub> particles at different weight percentages for automobile parts and sports goods applications.

## II. Material and Methodology

GF-SA reinforced epoxy composites were fabricated using Al<sub>2</sub>O<sub>3</sub> (1000 mesh, M.W. 101.96 g/mol, Sisco Research Laboratories Pvt. Ltd., Maharashtra, India) and SiC (1200 mesh, M.W. 40.096 g/mol, SRL Pvt. Ltd., Maharashtra, India) particulates with a 1200-mesh size), epoxy resin (LY 556, 1.026 gm/cc at 25°C, ASES Chemical Works, Rajasthan, India) and woven E-glass fiber. The process involved stirring the epoxy (60 wt. %) in a beaker at 80°C and 400 rpm for 30 minutes, followed by the gradual addition of SiC/Al<sub>2</sub>O<sub>3</sub> at the same temperature and stirring conditions for 4 hours to achieve a homogenous mixture. Different concentrations of SiC/Al<sub>2</sub>O<sub>3</sub> (0%, 2%, 4%, and 6% by weight) were added as per specifications. Furthermore, the curing agent HY951 (ASES Chemical Works, Rajasthan, India) was combined with the epoxy composite at a 1:10 ratio, following the manufacturer's recommendation. The interior surface of the bottom mold sheet received a uniform application of silicone spray. Epoxy resin was then evenly spread across the mold sheet using a brush, and GF was placed on top. A roller was used to eliminate air pockets and excess resin, applying gentle pressure during the process. This sequence was repeated until eight layers of glass fiber were stacked to achieve a thickness of 5 mm. The top mold sheet, treated with silicone, was placed over the assembly. The composite was subjected to a pressure of 4 MPa at 120 °C for 10 minutes within a compression molding press. After curing at room temperature for 24 hours, the mold was opened, and the composite part was carefully removed. A schematic diagram illustrating the fabrication process of the GF-SA reinforced epoxy composites was depicted in a figure1.

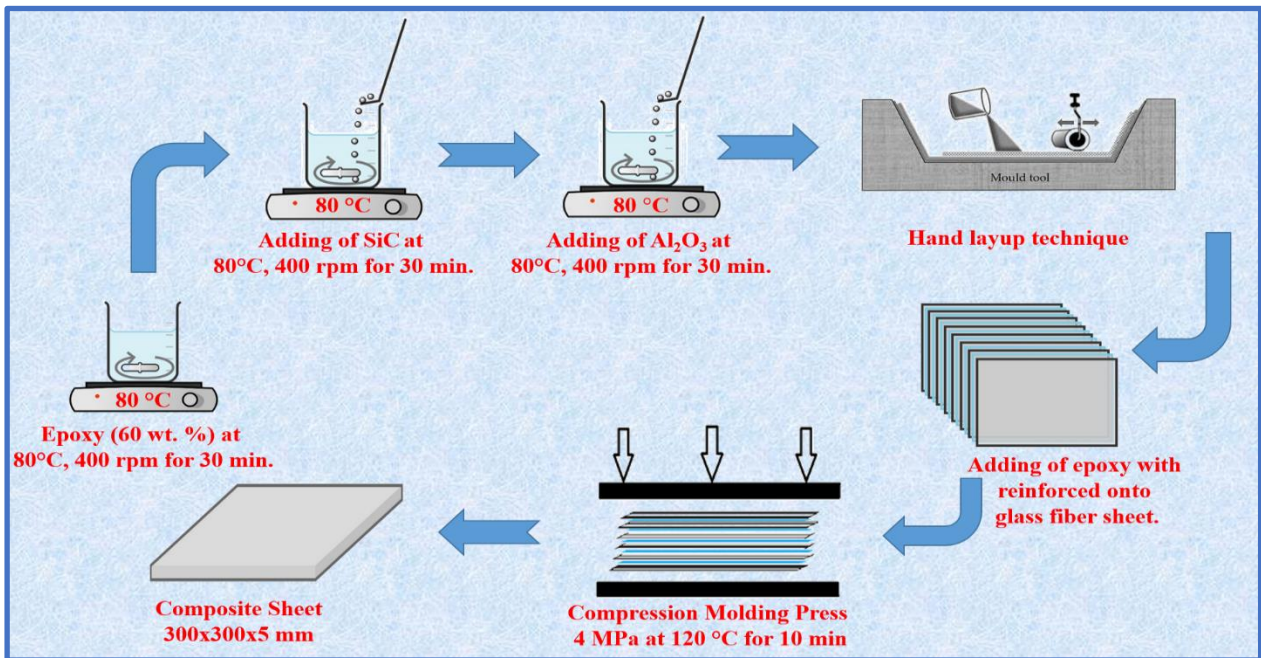


Figure 1: Schematic diagram illustrating the fabrication process of the GF-SA reinforced epoxy composites.

Table 1: The composites' names and configurations.

Name of Composites	Title	Composition of specimen
Epoxy/GF	GF-0SA	Epoxy (60 wt.%) + Fixed GF
Epoxy/GF/SiC:Al <sub>2</sub> O <sub>3</sub> (2:2)	GF-2SA	Epoxy (60 wt. %) + Fixed GF +SiC: Al <sub>2</sub> O <sub>3</sub> (2:2 wt. %)
Epoxy/GF/SiC:Al <sub>2</sub> O <sub>3</sub> (4:4)	GF-4SA	Epoxy (60 wt. %) + Fixed GF +SiC: Al <sub>2</sub> O <sub>3</sub> (4:4 wt. %)
Epoxy/GF/SiC:Al <sub>2</sub> O <sub>3</sub> (6:6)	GF-6SA	Epoxy (60 wt. %) + Fixed GF +SiC: Al <sub>2</sub> O <sub>3</sub> (6:6 wt. %)

### III. Experiments

#### 3.1 Density Measurement Test

Density represents a crucial physical characteristic of composite materials. The preference for low-density composites is attributed to their cost-effectiveness in production. Composite density is contingent upon the proportions of fiber filler and epoxy resin used. To assess composite density, the widely adopted method is based on Archimedes' principle. According to Archimedes' principle, "when an object is immersed, either partially or completely, in a fluid, an upward buoyant force is exerted on the object, which is equivalent in magnitude to the weight of the displaced fluid." To conduct the density test, specimens are cut into dimensions of 40 x15 x 4±1 mm from the composite sheet, which is shown in fig. 2 (a). Density can be calculated using the following formula:

$$\text{Density} = \frac{W_{SAa} \times \sigma_{SAw}}{W_{SAa} - W_{SAw}} \quad (1)$$

Where,  $W_{SAw}$  = The mass of GF – SA reinforced epoxy composite in DI water.

$W_{SAa}$  = The mass of GF – SA reinforced epoxy composite in ambient.

$\sigma_{SAw} = 0.998 \frac{gm}{cc}$  at NTP, density of DI water.

#### 3.2 Moisture Content (MC) Test

The moisture content test provides insight into the water content within the composites. This is accomplished by placing the specimens in an oven at a specified temperature until a consistent weight is achieved. Determining the moisture uptake is essential because fibers are particularly sensitive to moisture and humidity. It also serves as a crucial parameter for composite applications. The test is conducted following the mass fraction method.

To perform this experiment in accordance with ASTM D570 standards, samples of dimensions 20 x 20 x 4±1 mm are initially weighed and then subjected to 24 hours of drying (80 °C) in an oven until they reach a stable mass. The stabilization period depends on several factors, including the material type, quantity, and condition. Once this steady mass is achieved, the samples are reweighed. The moisture content can be calculated using the following formula:

$$\text{Moisture Content} = \frac{W_{MCSAi} - W_{MCSAf}}{W_{MCSAf}} \times 100 \quad (2)$$

Where,  $W_{MCSAi}$  = Weight of the GF – SA reinforced epoxy composite, before drying .  
 $W_{MCSAf}$  = Weight of GF – SA reinforced epoxy composite, after drying.

### 3.3 Water Absorption (WA) Test

Water absorption is measured using a weight percentage approach following ASTM D570 guidelines. The specimens for the WA test are sized at 20 x 20 x 4±1 mm, which is shown in fig. 2 (a). These specimens undergo drying in a hot air oven at 80°C for 24 hours to remove any moisture. Afterward, the weight of each dried sample is recorded before immersing them in water for 24 hours. Following the soaking period, the specimens are taken out, and their weights are measured again. The calculation can be performed using the equation provided below.

$$\text{Water Absorption} = \frac{W_{WASAf} - W_{WASAi}}{W_{WAbfi}} \times 100 \quad (3)$$

Where,  $W_{WASAf}$  = Weight of GF – SA reinforced epoxy composite after immersion.  
 $W_{WASAi}$  = Weight of GF – SA reinforced epoxy composite before immersion.

### 3.4 Linear Swelling Test

Linear swelling provides insight into changes in thickness, width, or length of materials. Linear swelling is assessed using the thickness/width/length percentage method. In accordance with ASTM D570 standards, the specimens for the linear swelling test are sized at 20 x 20 x 4±1 mm, which is shown in fig. 3 (a). The process involves placing these specimens in a hot air oven at 80°C for 24 hours to eliminate moisture. Afterward, the length/thickness/width of each dried sample is measured. Subsequently, the specimens are immersed in water for a 24-hour duration, then removed for re-measurement of their length/thickness/width. The formula below can be utilized to determine the extent of linear swelling.

$$\text{Linear Swelling} = \frac{L_{SAf} - L_{SAi}}{L_{SAi}} \times 100 \quad (4)$$

Where,

$L_{SAf}$  = Measurement of length, thickness and width of GF – SA sample, after immersion.  
 $L_{SAi}$  = Measurement of length, thickness and width of GF – SA sample, before immersion.

### 3.5 Flammability

The current experiment followed the ASTM 635 standard, utilizing specimens measuring 125 x 13 x 4±1 mm, as shown in fig. 4 (a). Each specimen was subdivided into three sections, marked at a 25 mm



distance from both free ends. Placed horizontally, each specimen's transverse axis was inclined at 45°. The flame front was positioned at the free edge of the specimen for a duration of 30 seconds. The stopwatch was initiated as the fire reached the 25-mm mark, and the time was recorded until it reached the 100-mm mark. The burning rate, expressed in mm/min, was determined by dividing the burned length by the recorded time. The remaining mass was weighed after removing the ashes to calculate the mass loss rate.

### 3.6 Mechanical Characterizations

The tensile and flexural test are conducted under ambient conditions (24±2°C, 40-45%) using the universal testing machine (UTM, Instron1195) on flat specimens in accordance with ASTM D3039-76 (150 x 20 x 4±1 mm) and D2344-84 (150 x 20 x 4±1 mm) respectively. All specimens with varying weight percentages of Al<sub>2</sub>O<sub>3</sub>/SiC (1:1) are subjected to uni-axial loading at a crosshead speed of 4 mm/min during the tensile and flexural test. The gauge length is set at 50 mm and 60 mm for each tensile and flexural test respectively. Three replicas of each sample are tested, and their mean value along with the standard deviation (S.D) is calculated for analysis.

The izod impact and Shore D hardness test for GF-SA composites were conducted under ambient conditions (24±2°C, 40-45%) on flat specimens in accordance with ASTM D 256 standards, with dimensions of 65 mm x 13 mm x 3.2 mm and featuring a 2.5 mm V-shaped notch and ASTM D2240, applying the load for 15 seconds respectively. Similar to the previous tests, three replicas are obtained for each sample, and the results are represented as mean ± standard deviation (S.D).

### 3.7 Microscopic Structure Analysis

Nova Nano FE-SEM 450 (FEI) is used for ultra-high resolution and precise scanning and also give information in nanometer scale. Scanning electron microscope is used for study of surface morphologies of tensile and flexural tested epoxy composites surfaces for determined the mode of material removal from surface. Nova Nano FE-SEM 450 (FEI) gives optical detection by using beam deceleration pass through lens. Scanning electron microscope can give resolution 1000x at 20 kV under pressure of 150 Pa. The size of specimens take as a 25 mm x 25 mm x 4±1mm for SEM test.

## IV. Experiments

### 4.1 Evaluation of Density Measurement Test.

Density serves as a crucial physical property in composites, with a preference for low-density materials owing to reduced production costs. The composite density is influenced by factors such as the quantity of resin (epoxy) as the polymeric matrix, woven E glass filler as reinforcement, and SiC/Al<sub>2</sub>O<sub>3</sub> as particulates.

Figure 2(b) illustrates the density graph concerning SiC/Al<sub>2</sub>O<sub>3</sub> particulates in WE-GFRE composites. WE-GFRE composite attains the highest density value at 2.696±0.020 g/cm<sup>3</sup>, attributed to enhanced bonding between the epoxy matrix and GF, along with minimized void formation. The GF-2SA reinforced composite exhibits lower density compared to others because of the formation of voids. The formation of voids is associated with the entrapment of air bubbles within the epoxy matrix, vapor formation during the resin and hardener curing process, and residual solvents. Additionally, difficulties in achieving complete wetting of the fiber by the resin after SiC/Al<sub>2</sub>O<sub>3</sub> particle mixing contribute to voids. Further examination from Figure 2 (b), it is evident that GF-4SA and GF-6SA reinforced composites show increase in density, attributed to the heightened density of SiC/Al<sub>2</sub>O<sub>3</sub> particulates within these composites.

### 4.2 Evaluation of Moisture Content Test.

Storage conditions play an important role in moisture content (MC). MC of composites depends on amount of resin (epoxy) as PMC material, WE-GF as reinforcement and SiC/Al<sub>2</sub>O<sub>3</sub> as particulates. In Fig. 2(c), the graph illustrates the percentage of moisture content (MC) compared to GF-SA reinforced UGC CARE Group-1

epoxy composites. WE-GFRE composite exhibits the highest percentage of MC at  $0.901 \pm 0.085\%$ , attributed to the presence of free -OH groups within both the epoxy matrix and FG.

### 4.3 Assessment of Water Absorption Test.

Performance and integrity of the composites determine by water absorption. WA in composites is dependent on fiber loading, type of particulates, area of small the expose surface, filler/particulate loading, surface protection. Void content, orientation of fibers, diffusivity, and permeability of fiber and hydrophilicity of components. In Fig. 2(d), the graph illustrates the percentage of WA concerning GF-SA reinforced epoxy composites. WE-GFRE composite exhibits the highest percentage of WA at  $1.499 \pm 0.275\%$ , attributed to poor compatibility between the epoxy matrix and GF. Subsequently, in Figure 2(d), it's noted that the WA percentage in GF-2SA reinforced epoxy composites experiences a sudden decrease, likely due to the presence of SiC particulates. Moreover, the WA percentage increases from 2 to 6 wt. % in GF-SA reinforced epoxy composites due to the inclusion of  $Al_2O_3$  particulates.

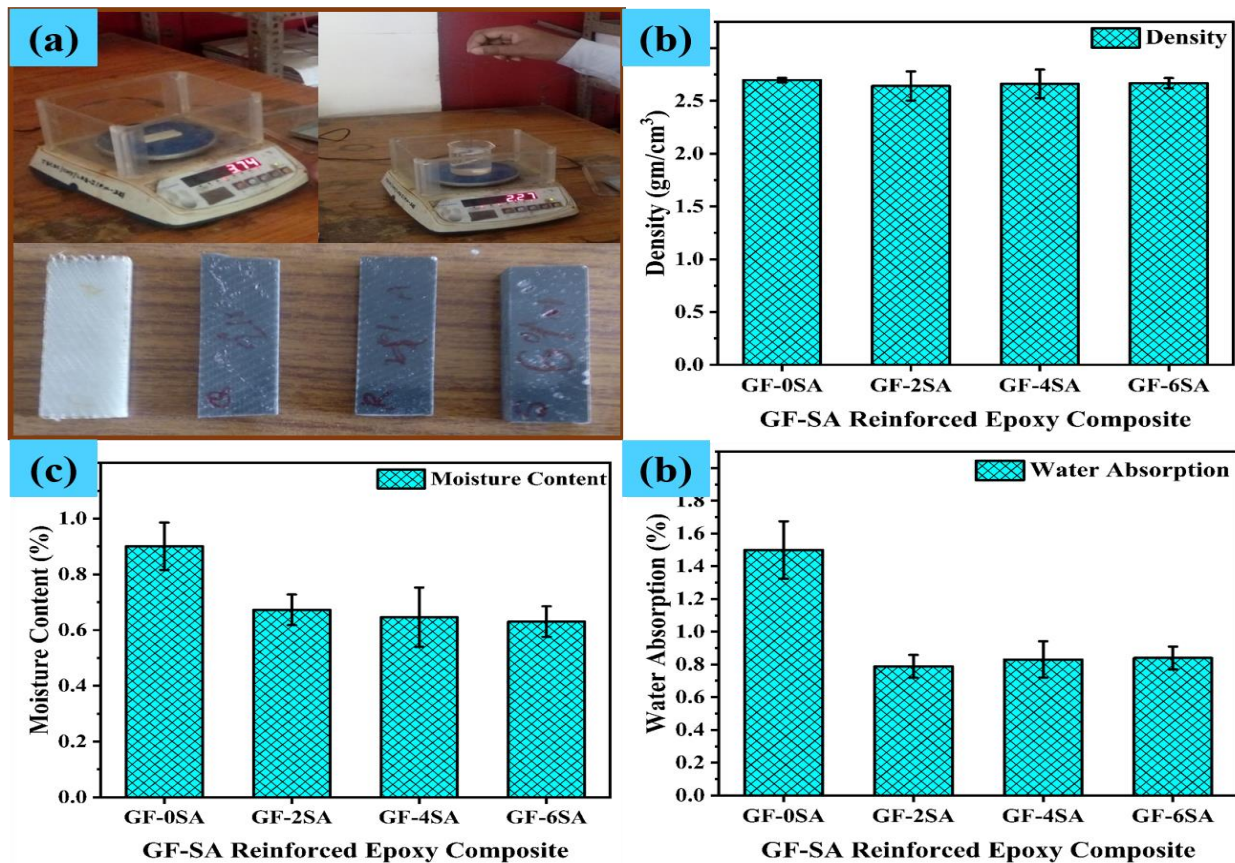


Figure 2: (a) Photograph of specimens for density test. Comparison of (b) density (c) moisture content (d) water absorption of GF-SA reinforced epoxy composites.

### 4.4 Assessment of Linear Swelling Test.

Dimensional stability of the physical property affected final performance of composites because presences of moisture content may change the size of specific product during operation. The change in thickness/width/length was measured to determine the linear swelling in figure 3 (b), the graph illustrates the percentage of thickness swelling (TS) in GF-SA reinforced epoxy composites. WE-GFRE composite shows the highest TS percentage at  $27.131 \pm 0.142\%$ , which can be attributed to poor compatibility between the epoxy matrix and GF (indicating a correlation between TS and WA). Subsequently, figure 3(b) indicates a sudden decrease in the TS (%) in GF-2SA reinforced epoxy composites, which could be attributed to the presence of SiC particulates.

Figure 3(b) indicates an increase in the TS (%) values for GF-4SA and GF-6SA composites, attributed to the rising percentage of weight of  $Al_2O_3$  particulate. Similarly, Figure 3(c) and Figure 3(d) reveal an increase in the values of WS (%) and LS (%) for GF-4SA and GF-6SA composites, corresponding to an increment in the percentage of weight of  $Al_2O_3$  particulate.

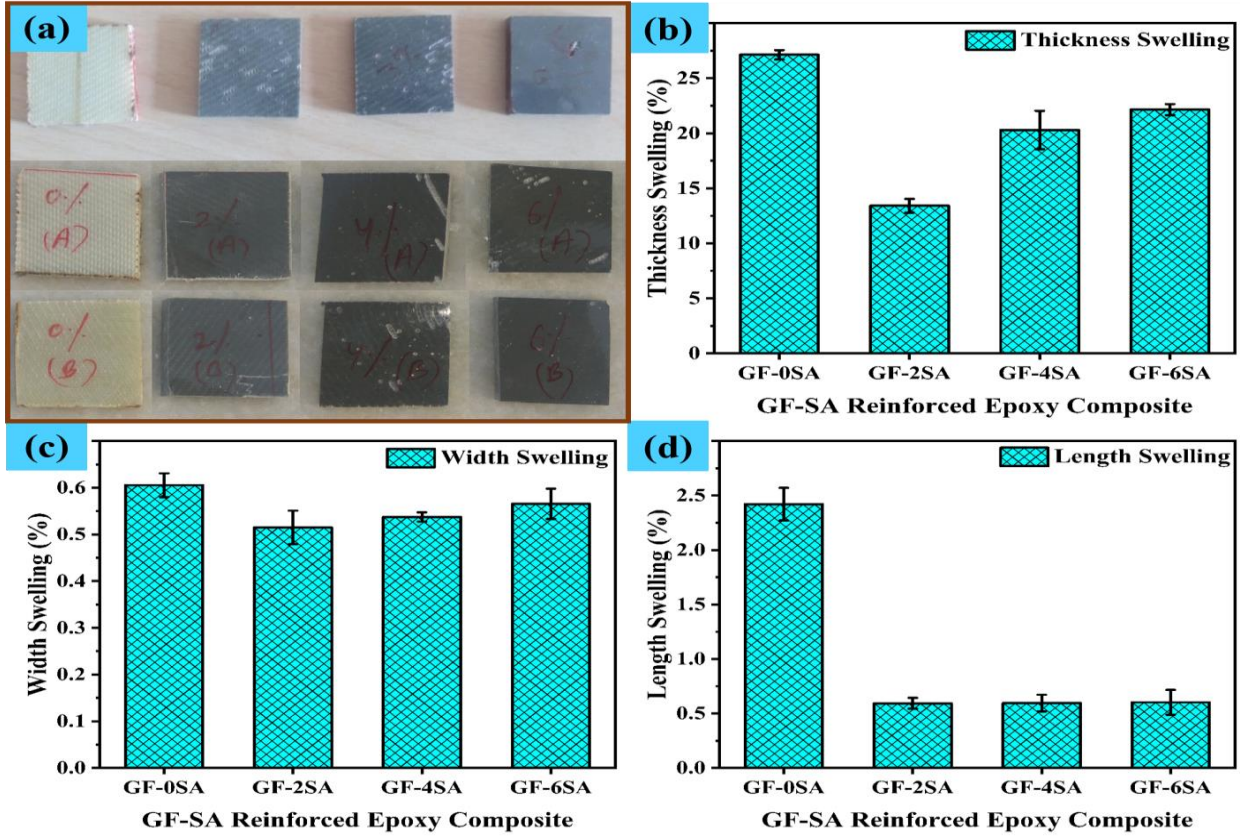


Figure 3: (a) Photograph of specimens for swelling test. Comparison of (b) thickness swelling, (c) width swelling and (d) length swelling of GF-SA reinforced epoxy composites.

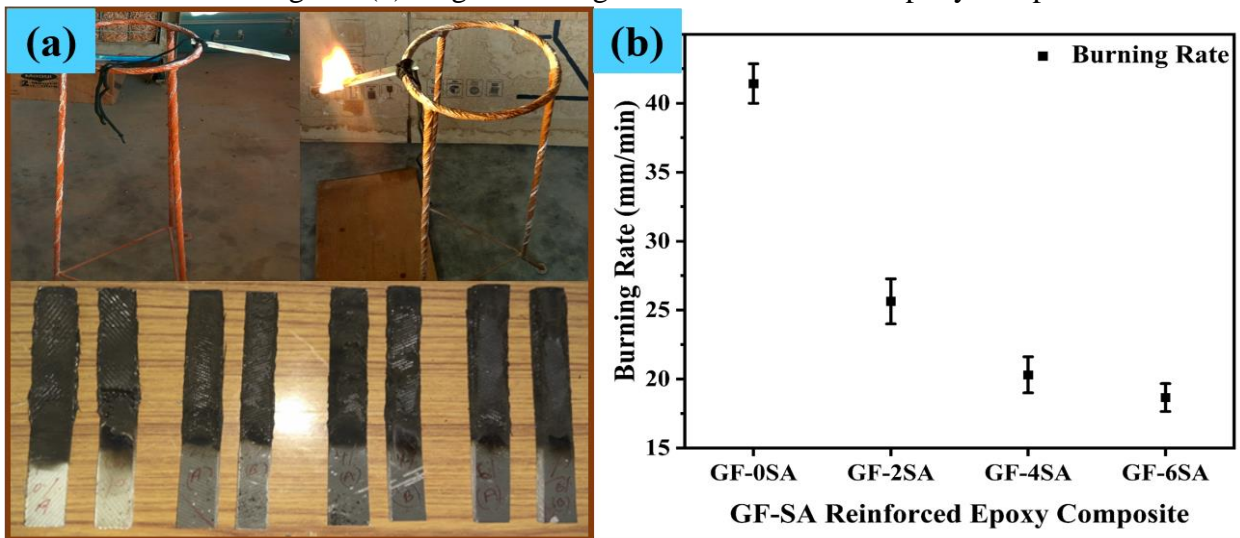


Figure 4: (a) Photograph of specimens for flammability test. (b) Comparison of burning rate of GF-SA reinforced epoxy composites.

#### 4.5 Flammability Test

Figure 4 (b) illustrates the burning rate of GF-SA reinforced epoxy composite specimens in length per unit minute. The flammability test reveals that the 'GF-6SA' specimen exhibits the lowest burning rate in length per unit minute, attributed to the increased presence of ceramic in the composites.

#### 4.6 Study of Tensile Test

The mechanical tensile properties of GF-SA-reinforced epoxy composites are illustrated in figure 5 (a), 5(b), 5 (c) and 5(d). The tensile strength property of composites is commonly influenced by both the GF content and the strength of GF. The ultimate tensile strength of a material is represented by the ratio of the maximum load applied to the material to the initial cross-sectional area of the test specimen. Figure 5(b) presents the curves depicting ultimate tensile strength ( $\sigma_t$ ) and yield strength ( $\sigma_y$ ) in relation to GF-SA reinforced epoxy composites.

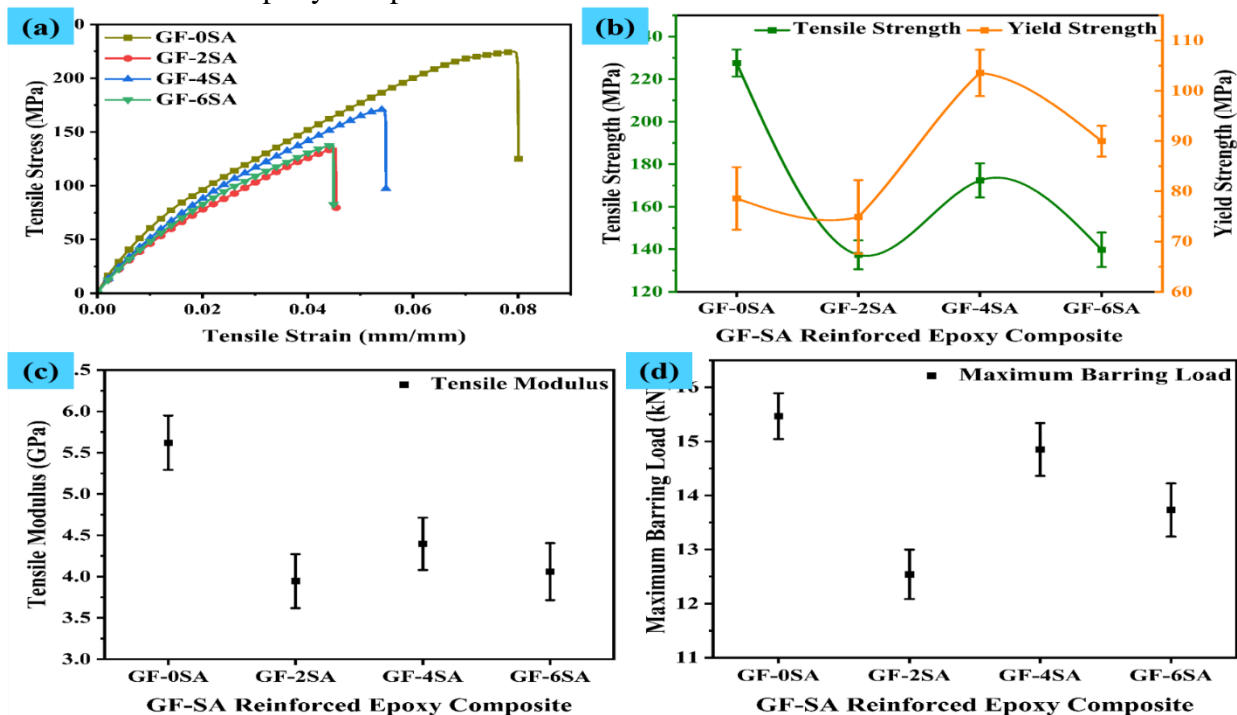


Figure 5: GF-SA reinforced epoxy composites (a). Tensile stress Vs Tensile strain (b). Tensile strength and Yield strength Vs SiC/Al<sub>2</sub>O<sub>3</sub> (1:1) wt. %. (c). Tensile Modulus Vs SiC/Al<sub>2</sub>O<sub>3</sub> (1:1) wt. %. (d). Maximum barring load Vs SiC/Al<sub>2</sub>O<sub>3</sub> (1:1) wt. %.

WE-GFRE composite exhibits  $\sigma_t$  of  $227.55 \pm 6.35$  MPa and  $\sigma_y$  of  $78.58 \pm 6.22$  MPa, attributable to the enhanced bonding strength between the epoxy matrix and GF. Subsequently, both  $\sigma_t$  and  $\sigma_y$  experience a sudden decrease on account of the presence of SiC/Al<sub>2</sub>O<sub>3</sub> (1:1) particles, which act as barriers hindering the transfer of stress between points and result in poor bonding strength among the epoxy matrix, SiC, Al<sub>2</sub>O<sub>3</sub>, and GF. Figure 5(b) shows a subsequent increase in both  $\sigma_t$  and  $\sigma_y$  for GF-2SA to GF-6SA composites, which can be attributed to the enhanced transfer of stresses between points within the composite.

WE-GFRE composite exhibits the highest tensile modulus ( $E_t = 5.621 \pm 0.329$  GPa) and maximum barring load (MBL =  $15.468 \pm 0.423$  kN), attributable to the superior bonding strength between the epoxy matrix and GF. Figure 5(c) and 5(d) show an increase in both  $E_t$  and MBL for GF-2SA to GF-6SA composites, attributed to the relatively lower strain rates of GF-SA composites and an increase in stress transfer between points within the composite, respectively.

#### 4.7 Study of Flexural test

The flexural properties of composites are commonly influenced by both the GF content and the strength of the GF. In the flexural test, the specimen is positioned between two point supports, and a

load is applied at the top layer or the midpoint of the specimen. This setup induces compressive stress on the upper fiber and tensile stress on the lower fiber of the specimen. The observations from the flexural tests conducted on four GF-SA composites are presented in figure 6 (a) and 6 (b).

The WE-GFRE composite exhibits flexural strength ( $\sigma_f = 201.887 \pm 8.174$  MPa) and flexural modulus ( $E_f = 14.083 \pm 0.585$  GPa) attributed to enhanced bonding strength between the epoxy matrix and GF. Figures 6 (a) and 6 (b) indicate an increase in both  $\sigma_f$  and  $E_f$  for GF-2SA to GF-6SA composites, on account of the excellent compatibility between the epoxy matrix and GF and the relatively lower strain rates of GF-SA composites, respectively.

#### 4.8 Study of Impact test

Izod Impact Test of four sample of WE-GFRE composite are carried out at ambient conditions. It is observed from figure 6 (c) that the value of the impact strength (23.45 J/m) at 4 wt. % SiC/Al<sub>2</sub>O<sub>3</sub> (1:1) is superior to other composites. The reason behind for this is the better bonding strength between epoxy matrix and GF.

#### 4.9 Study of Shore D Hardness

Hardness of GF-SA reinforced epoxy composite are measured at ambient condition using shore D hardness. Figure 6 (d) shows that the value of the hardness is increased with increasing weight percentage of SiC/Al<sub>2</sub>O<sub>3</sub> (1:1) in GF-SA composite due to the widespread presence of SiC/Al<sub>2</sub>O<sub>3</sub>. The reinforcement of SiC/Al<sub>2</sub>O<sub>3</sub> into matrix to prevent formation of void and pores into composites as result better bonding occur in between matrix and GF.

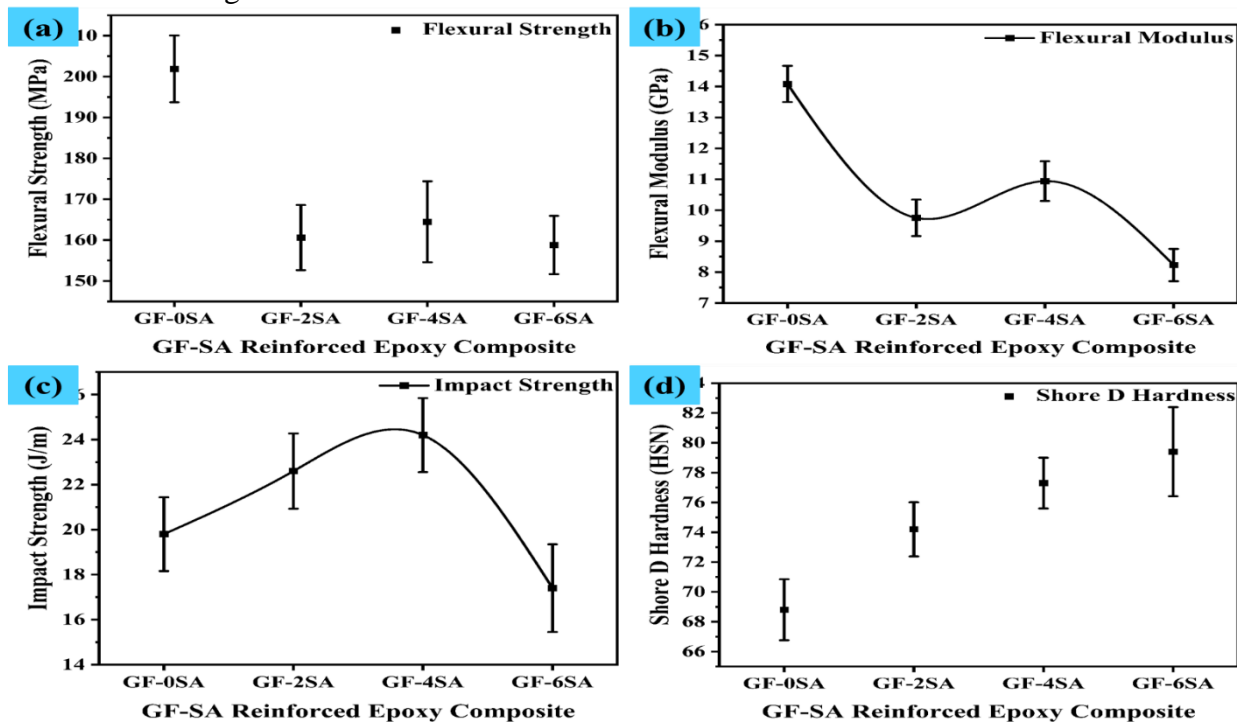


Figure 6: GF-SA reinforced epoxy composites (a). Flexural Strength Vs SiC/Al<sub>2</sub>O<sub>3</sub> (1:1) wt. %. (b). Flexural Modulus Vs SiC/Al<sub>2</sub>O<sub>3</sub> (1:1) wt. %. (c). Impact strength Vs SiC/Al<sub>2</sub>O<sub>3</sub> (1:1) wt. %. (d). Shore D hardness Vs SiC/Al<sub>2</sub>O<sub>3</sub> (1:1) wt. %.

#### 4.10 Microscopic Structure Analysis

SEM is employed to examine the surface topographies of GF-SA composite specimens, specifically focusing on the tensile and flexural behaviors, to determine the mode of material removal from the surface. Figure 7 and figure 8 illustrate a fracture section of the tensile and flexural specimen surfaces observed under SEM, respectively.

The GF-SA composite specimens exhibit a high percentage of epoxy, contributing to improved wetting of GF, a better interface between GF and the matrix, and the embedding of GF into the epoxy matrix. The FE-SEM analysis in Figure 7 (a), Figure 7 (c), and Figure 7 (d) also indicates that different layers of GF are effectively encapsulated by distinct layers of epoxy. As results, robust bond and favorable interfacial adhesion between the GF and epoxy matrix facilitate efficient load transfer, ensuring a uniform stress distribution. This compatibility promotes effective stress transmission and contributes to the enhancement of mechanical properties of GF-SA composite. During the tensile and flexural tests, Figure 7 (b) and Figure 8 (b) depict instances where some GF is pulled out from the epoxy matrix, and certain fibers break in both longitudinal and transverse directions, respectively. Fiber pull-out suggests the effectiveness of the fiber in maintaining adhesion within the matrix. Additionally, it is examined that the tensile and flexural behaviors of GF-SA composites decline due to the agglomeration between filler around the matrix, hindering the proper curing of the composite.

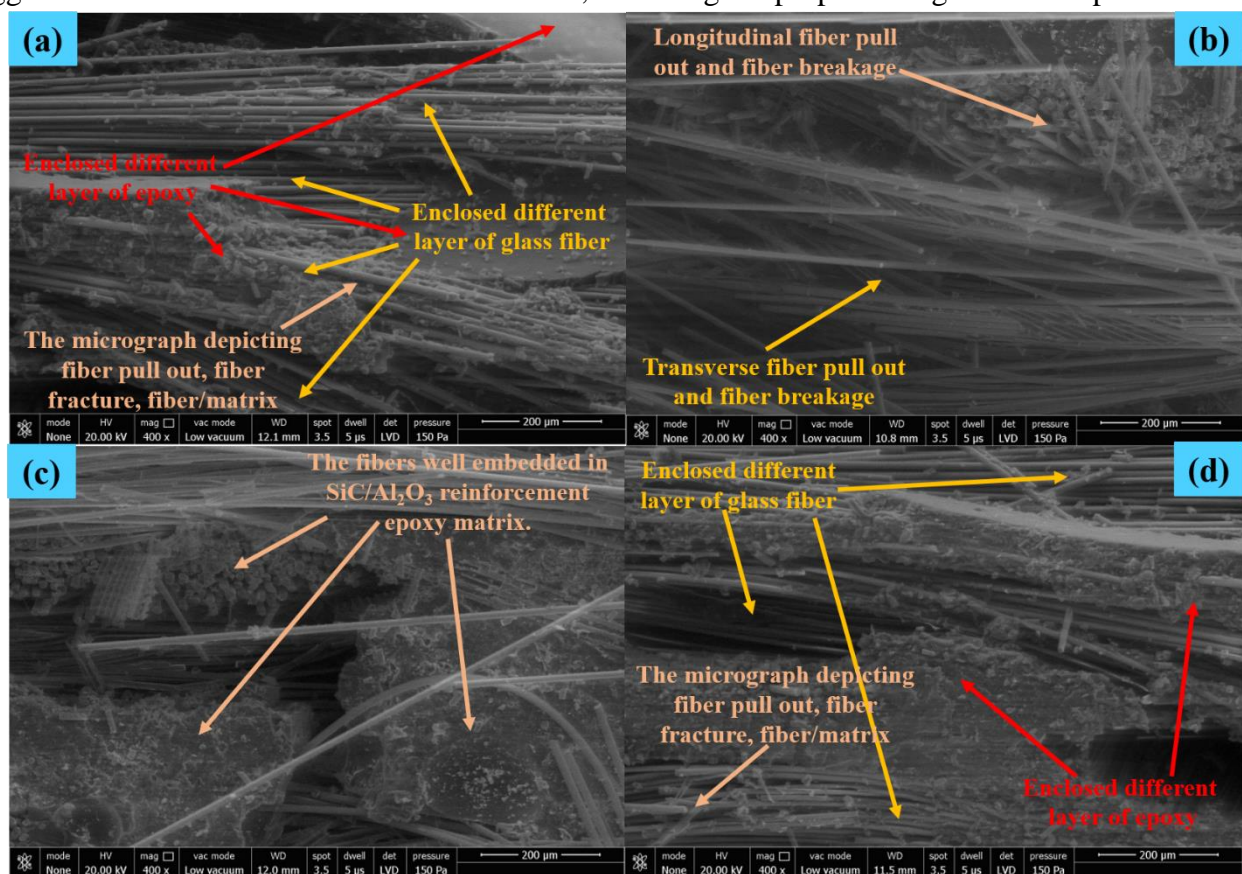


Figure 7: FE-SEM analysis of tensile fracture (a). GF-0SA, (b) GF-2SA, (c) GF-4SA, and (d) GF-6SA reinforced epoxy composites.

The SEM analysis of the flexural behaviors of GF-SA composites in Figure 8 (a) and figure 8 (c) reveal that the fibers within the array display twisting on the fractured surface in both longitudinal and transverse directions. This suggests that the composite specimens possess a higher degree of fiber alignment under stress, resulting in a better fiber efficiency factor and consequently, enhanced mechanical strength. Figure 8(d) shows de-bonding of GF/matrix, rupture of fiber and imprint of GF in epoxy matrix on account of weak interaction between GF and epoxy matrix, which is negativity impact on mechanical properties of GF-6SA composites.

## V. Conclusion

The experimental and analytical assessment of GF-4SA reinforced epoxy composite has revealed optimum physical properties, including a density of  $2.661 \pm 0.135 \text{ g/cm}^3$ , an absorption percentage of  $0.646 \pm 0.106\%$ , a moisture content percentage of  $0.830 \pm 0.111\%$ , and minimal linear swelling in all

dimensions, which may be due to the presence of voids, and the presence of micro cracks within the composite. Mechanical testing of GF-4SA reinforced epoxy composite exhibits better tensile, flexural, impact and harness properties. The SEM analysis of the tensile and flexural tests indicates that robust bond and favorable interfacial adhesion between the GF and epoxy matrix facilitate efficient load transfer, ensuring a uniform stress distribution.

Existing literature reviews support the notion that micro-particle composites exhibit lower water absorption and superior dimensional stability, which is consistent with the findings of this study. This reaffirms the accuracy and reliability of the research. Hence, it can be concluded that the obtained composites are well-suited for use in automobile parts and sports goods, given their enhanced physical and mechanical properties.

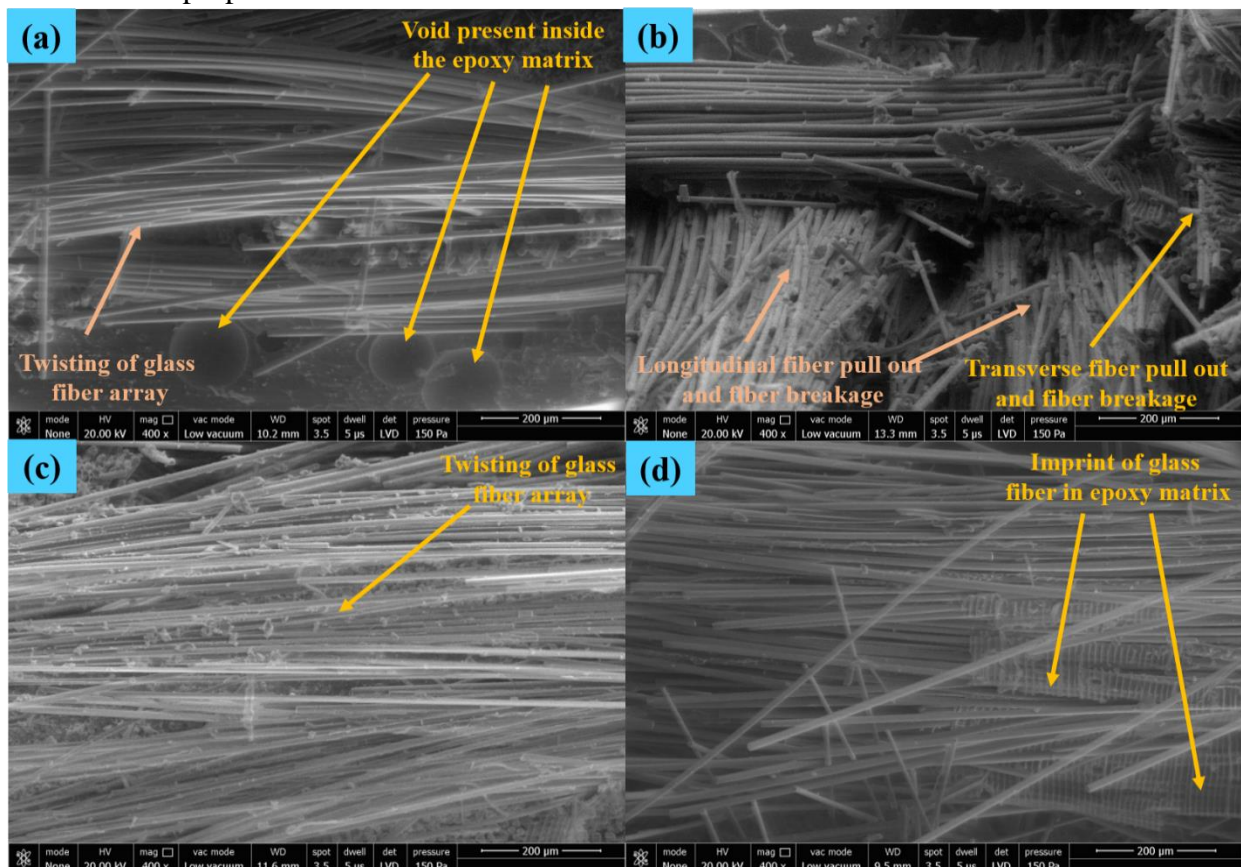


Figure 8: FE-SEM analysis of flexural fracture (a). GF-0SA, (b) GF-2SA, (c) GF-4SA, and (d) GF-6SA reinforced epoxy composites.

## References

- [1] E. Kosedag, R. Ekici, N. Yildiz, U. Caliskan, Effect of SiC and graphene nanoparticles on the mechanical properties of carbon fiber-reinforced epoxy composites, *Polymer Composites*. (2023). <https://doi.org/10.1002/pc.27720>
- [2] S. M. Shahabaz, P. Mehrotra, H. Kalita, S. Sharma, N. Naik, D. J. Noronha, N. Shetty, Effect of Al<sub>2</sub>O<sub>3</sub> and SiC Nano-Fillers on the Mechanical Properties of Carbon Fiber-Reinforced Epoxy Hybrid Composites, *Journal of Composites Science*. 7(4) (2023) 133. <https://doi.org/10.3390/jcs7040133>
- [3] S. Sathish, K. Kumaresan, L. Prabhu, S. Gokulkumar, N. Karthi, N. Vigneshkumar, Experimental investigation of mechanical and morphological properties of flax fiber reinforced epoxy composites incorporating SiC and Al<sub>2</sub>O<sub>3</sub>, *Materials Today: Proceedings*. 27 (2020) 2249-2253. <https://doi.org/10.1016/j.matpr.2019.09.106>



- [4] M. D. Kiran, H. K. Govindaraju, T. Jayaraju, Evaluation of mechanical properties of glass fiber reinforced epoxy polymer composites with alumina, titanium dioxide and silicon carbide fillers, *Materials Today: Proceedings*. 5(10) (2018) 22355-22361.  
<https://doi.org/10.1016/j.matpr.2018.06.602>
- [5] N. Singh, R. Singh, I. P. S. Ahuja, Thermomechanical investigations of SiC and Al<sub>2</sub>O<sub>3</sub>-reinforced HDPE, *Journal of Thermoplastic Composite Materials*. 32(10) (2019) 1347-1360.  
<https://doi.org/10.1177/0892705718796544>
- [6] O. T. Sanya, B. Oji, S. S. Owoeye, E. J. Egbochie, Influence of particle size and particle loading on mechanical properties of silicon carbide-reinforced epoxy composites, *The International Journal of Advanced Manufacturing Technology*. 103(9-12) (2019) 4787-4794.  
<https://doi.org/10.1007/s00170-019-04009-1>
- [7] P. K. Gupta, R. Sharma, G. Kumar, Impact of water particles on fly ash-filled E-glass fiber-reinforced epoxy composites, In *Advanced Materials and Manufacturing Processes*. (pp. 257-267) (2021) CRC Press.
- [8] R. Sharma, P. K. Gupta, Synthesis and chemical resistance of aluminum oxide and silicon carbide (1:1) filled Bi-Directional woven E-glass fiber reinforcement epoxy polymer composites, *Materials Today: Proceedings*. 62 (2022) 767-772. <https://doi.org/10.1016/j.matpr.2022.03.673>
- [9] R. Sharma, D. Sharma, Synthesis and experimental investigation of physical behavior of coconut shell particular and walnut shell particular filled epoxy polymer composites, *Materials Today: Proceedings*. (2023). <https://doi.org/10.1016/j.matpr.2023.02.455>
- [10] N. M. Mathur, Yashpal, B. Pratap, Development and evaluation of physical properties of PLA matrix composites reinforced with SCB/CF fiber, *Proceedings of the Institution of Mechanical Engineers, Part C: Journal of Mechanical Engineering Science*. 09544062231179991 (2023).  
<https://doi.org/10.1177/09544062231179991>